Plasmonics-enhanced and optically modulated delivery of gold nanostars into brain tumor

Hsiangkuo Yuan[a,†], **Christy M. Wilson**[b,†], **Jun Xia**[c,†], **Sarah L. Doyle**[d,†], **Shuqin Li**[b], **Andrew M Fales**[a], **Yang Liu**[e], **Ema Ozaki**[d], **Kelly Mulfaul**[d], **Gabi Hanna**[f], **Gregory M. Palmer**[f], **Lihong V. Wang**[c], **Gerald A. Grant**[b], and **Tuan Vo-Dinh**[a,e]

[a]Department of Biomedical Engineering, Fitzpatrick Institute for Photonics, Duke University, Durham, NC 27708, USA [b]Department of Surgery, Division of Neurosurgery, Duke University Medical Center, Durham, NC 27710, USA [c]Department of Biomedical Engineering, Washington University in St. Louis, St. Louis, MO 63130, USA [d]Department of Clinical Medicine, School of Medicine, Trinity College Dublin, Dublin 2 and the National Children's Research Centre, Our Lady's Children's Hospital, Crumlin, Dublin 12, Ireland [e]Department of Chemistry, Duke University, Durham, NC 27708, USA [f]Department of Radiation Oncology, Duke University Medical Center, Durham, NC 27710, USA

Abstract

Plasmonics-active gold nanostars exhibiting strong imaging contrast and efficient photothermal transduction were synthesized for a novel pulsed laser-modulated plasmonics-enhanced brain tumor microvascular permeabilization. We demonstrate a selective, optically modulated delivery of nanoprobes into the tumor parenchyma with minimal off-target distribution.

In the pursuit of better treating medically intractable malignant glioblastoma, novel strategies designed to overcome the physiological obstacles imposed by the blood brain-tumor barrier (BBTB) have been shown to facilitate the delivery of therapeutic agents into the tumor parenchyma.[1, 2] Strategies exploiting either biological entities (*e.g.,* immunotherapy, gene therapy) or transient physical blood-brain barrier (BBB) disruption (*e.g.,* high-intensity focused ultrasound [HIFU]) have recently shown significant preclinical progress.[3, 4] Novel platforms based on nanotechnology have also emerged to treat neurological malignancies due to their superior pharmacokinetic profiles than conventional drugs.[5, 6] Targeted brain tumor nano-drug delivery can be achieved by exploiting their enhanced permeation and retention (EPR) effect as well as utilizing them as molecular "Trojan horses" (*e.g.,* receptor-mediated transcytosis via transferrin, apolipoprotein, cyclic-RGD peptide, *etc.*). However, prior efforts have shown that with nano-drugs alone, the majority of systemically injected nanoparticles (NPs) remain in the reticuloendothelial system (RES; *e.g.,* liver, spleen, lymph node, *etc.*) whereas brain accumulation accounts for

Correspondence to: Tuan Vo-Dinh.

[†]These authors contributed equally.

less than 0.1 % of the injection dosage.[7, 8] Here, we develop a new strategy to increase the brain tumor accumulation by integrating nanotechnology (*e.g.* theranostics, targeted delivery) with selective BBTB permeation. We demonstrate that such strategy not only allows for nano-drug imaging and therapeutic response monitoring, but also induces transient BBTB permeation for use in enhanced nano-drug delivery with superior spatial and temporal specificity. As a result, image-guided BBTB permeabilization and controlled nano-drug delivery are achieved and will bring new insights to targeted brain tumor therapy.

Our strategy involves developing novel monolithic multifunctional NPs that features three functionalities: optical imaging contrast, photoactivated transducer, and therapeutic agent. Unlike three separated agents with distinct pharmakokinetic profiles, integrated design exhibits shared pharmacokinetic profile suitable for direct monitoring the delivery of therapeutic agent. Compared to conventional imaging methods (*e.g.*, MRI or ultrasound), optical methods also offer higher spatial and temporal resolution.[9] Hence, such an optical theranostic NP can be imaged and photoactivated under a single optical setup in high resolution.

In this study, NIR-responsive plasmonic gold nanostars (GNS) were used. Recently, NIR-responsive plasmonic gold NPs of various shapes (*e.g.,* shell, rod, cage, hollow sphere, star, *etc.*) have become one of the most promising theranostic agents designed for preclinical optical imaging and therapeutics.[10-13] Also, plasmonic gold NPs exhibit simple size/shape tunability, versatile surface chemistry, intrinsic optical property, and biocompatibility. Depending on their nanoscale sizes and shapes, they display strongly enhanced electromagnetic fields due to the so-called 'plasmonic effect', which produces unique intrinsic optical properties that can be exploited as imaging contrast and therapeutic agents without further coupling of dye or drug.[10, 12]

In particular, GNS not only have plasmon peaks in the NIR 'tissue optical window' range but also contain multiple sharp tips creating a "lightning rod" effect that further enhances the local surface plasmon; these unique optical properties bring forth strong surface-enhanced Raman scattering intensity (10^6 enhancement factor), large extinction coefficient (10^{9-10} M^{-1} cm^{-1}), enhanced two-photon photoluminescence (two-photon action cross section of 10^6 Goeppert-Mayer unit), and short lifetime (0.2 ns) for sensitive real-time imaging,[14, 15] as well as efficient photothermal transduction for photothermal therapy or photothermal-triggered drug release.[16-18] With these unique plasmonic features, GNS are potential multifunctional plasmonic NPs that allow for both high-resolution imaging evaluation of NP intratumoral distribution and image-guided photothermal-triggered BBTB permeabilization for controlled NP delivery.[10]

Here, GNS' plasmon maximum was tuned to 800 nm to match the laser excitation system for optimal two-photon photoluminescence response (Fig. 1A). The GNS surface was protected by PEGylation for reduced RES clearance and extended circulatory half-life. The final hydrodynamic size was around 80 nm (Fig. S1). When investigated *via* photoacoustic computer tomography (PACT) through intact scalp,[19] the photoacoustic (PA) signal rose instantly and then increased gradually before reaching a maximum at around half an hour (Fig. 1B). The intravascular PA intensity then slowly declined as GNS were cleared from

the RES or extravasated into tissues elsewhere. Measured through PACT, an extended circulatory half-life greater than 4 hours was found. Furthermore, due to its large extinction coefficient, high absorption-to-scattering ratio, and multiple thin branches favorable for heat generation, the GNS heat up quickly upon laser irradiation rendering it an efficient photothermal transducer (Fig. S1).[20]

To investigate the GNS intratumoral distribution with high spatial resolution, multiphoton microscopy (MPM) was employed through a cranial window chamber on orthotopic brain tumor animal models. Tumor xenograft in the cranium typically has smaller pore cutoff size than subcutaneous xenograft. Using dextran of various sizes, the pore size of the D270 glioma xenograft was found around 70-100 kDa (7∼9 nm; data not shown), which is smaller than that of the commonly used U87MG glioma xenograft;[21] D270 thus behaves closer than U87MG to actual human glioma. Due to GNS' intense two-photon photoluminescence signal and short fluorescence lifetime, subcellular resolution MPM imaging of GNS can be obtained using low laser energy (*e.g.,* 0.5∼1.5 mW at 800 nm) and fast scanning speed (*e.g.,* 2 μs/pixel). Since standard biodistribution quantification on a whole brain using elemental analysis (*e.g.,* ICP-MS) or whole-body imaging cannot distinguish intravascular or intraparenchymal accumulation, MPM complements whole-body imaging by offering a unique imaging tool with superior detection sensitivity and greater spatial/temporal resolution.

Fig. 1C illustrates a high-resolution depth-resolved *in vivo* cerebral microangiogram taken through a cranial window. Capillaries were clearly visible with minimal tissue autofluorescence background. Unlike commonly used intravascular contrast (*e.g.,* FITC-dextran) that undergoes significant signal decay in less than 30 minutes, the intravascular intensity of our GNS remained stable for hours without significant extravasation (Fig. S2), reflecting its intravascular stability inherited from inert gold and strong surface PEGylation. On a non-perfused mouse whole brain resected 3-hour post injection, GNS can be seen more prevalent in the tumor than the surrounding normal area (Fig. 1C,S3). On histology of perfused brains, GNS not only accumulated in the tumor vascular endothelial cells (ECs), but also selectively penetrated BBTB but minimally BBB to enter perivascular tumor parenchyma and tumor periphery (Fig. 1C,S4,S5). Tumor vessels appear larger in diameter but lower in density whereas distinctive GNS extravasation can be clearly seen. Long circulatory half-life superimposed on the EPR effect (fenestrated or gapped EC on capillary or venule) leads to EC accumulation and paracellular extravasation with possibly minimal true transcytosis.[22] Peripheral tumor accumulation of PEG-GNS is most likely due to the hyper-neovascularity along the tumor edge and interstitial fluid pressure gradient at the boundary that would attenuate GNS delivery deep into the tumor. Nonetheless, a great portion of PEG-GNS still accumulated in RES (Fig. S6). To further enhance the brain tumor GNS delivery and reduce off-target distribution, additional BBTB opening mechanism needs to be explored.

To date, many alternative delivery strategies have been investigated for systemically delivering NPs into brain parenchyma.[4, 23, 24] In particular, HIFU, which has been applied to increase BBB permeation by transiently disrupting the vascular integrity, has shown some progress in preclinical settings.[25] To improve the delivery specificity from HIFU

(millimeter-resolution), optical method featuring superior spatial control (micrometer-resolution) potentially allows for more specific delivery. Choi *et al.* recently reported optically modulated selective vascular permeabilization using a pulsed laser but required high laser power (300-2000 mW).[26] To reduce the laser burden while maintaining the optical selectivity, plasmonics-active NPs can be used to significantly enhance the laser-induced permeabilization effect. Ultrashort laser pulse interacting with plasmonics-active nanoparticles can lead to heating, stress wave release, or vapor bubble formation.[27, 28] GNS, by having plasmon absorption matching the excitation laser, high absorption-to-scattering ratio, and multiple thin branches favorable for heat generation,[20] can therefore be a strong candidate to enhance the laser-induced vascular permeabilization. Our study for the first time achieved a plasmonics-enhanced and optically modulated delivery of GNS into brain tumor under a much lower laser power (35 mW).

Exploiting GNS' plasmonic property, a locally triggered vascular permeabilization can be achieved through a cranial window *in vivo* at low NP dose (< 1 pmole) and laser power (35 mW; 14 W/cm^2) (Fig. 2), thus avoiding unwanted hemorrhagic infarction under high-power photothermal treatment (data not shown). The irradiation was performed within 10 minutes after PEG-GNS tail vein injection when most GNS were intravascular with little uptake in ECs or RES. After finding the tumor region, the laser irradiation was performed on the same multiphoton microscope. Immediately following the pulsed laser irradiation, some vasoconstriction and a minute focal extravasation was visible (Fig. 2B). 48-hour afterwards, extravasation could be seen in tumor vessels confined to the whole irradiated volume but not the surrounding tumor tissue (Fig. 2C-G). In normal brain, no apparent extravasation was found after the same irradiation (Fig. S7). Irradiating the brain tumor region using the same laser power but without GNS resulted in no observable extravasation of FITC-dextran (Fig. S8). The treatment was well tolerated with no sign of neurological disability over the next 2 days. Even though the tumor vascular pore size is much smaller than the 80-nm GNS, an apparent GNS permeation of 10-30 μm deep into tumor parenchyma is visible (Fig. 2C-E); the extravasation depth is much greater than that from merely EPR effect. It is of interest that the selective tumor vessel response may add another level of tumor targeting specificity. Although the irradiation is depth-limited in this study, it provides an unprecedented spatial selectivity for enhanced targeted GNS delivery in cortical tumor.

To understand this process, it is noteworthy to know that the impact of NP exposure could be derived from a combined physical, chemical, as well as immunological trigger that eventually affect the BBB or BBTB causing increased vascular permeability. The mechanism of this delayed regional BBTB permeabilization may possibly explained by short-term intravascular hyperthermia or energy burst that triggers a local inflammatory response exacerbating the already weakened tumor neovasculature whereas normal vessels were less vulnerable and did not show significant extravasation.[29] Hence, plasmonics-enhanced low-energy pulsed laser treatment may preferentially induce tumor vascular ECs inflammasome activation that enhances regional BBTB permeability.

To investigate the possibility of the immunological involvement using an *in vitro* system, we examined the cytotoxicity and inflammasome induction on bone marrow derived macrophages (BMDMs) upon exposure to PEG-GNS. The formation of the NLRP3-

inflammasome regulates the maturation of the proinflammatory cytokines (*e.g.,* interleukin 1β [IL-1β] and IL-18) in response to exogenous or endogenous danger signals during innate immunity. Here, PEG-GNS exposure to lipopolysaccharide (LPS)-primed macrophages resulted in the production of IL-1β and tumor necrosis factor α (TNFα) but not IL-6 (Fig. 3), implying that PEG-GNS do not induce a non-specific pan-inflammatory response. Rather, both TNFα and the inflammasome were activated related to NP concentration and incubation duration (Fig. S9); this is consistent with previous findings on different NPs (*e.g.,* silica, silver, polystyrene) suggesting a possible universal immunological impact from NPs.[30-32] Interestingly, although PEGylation can be used for reducing immunoclearance, PEGylated NP may still activate the inflammasome once being taken up a greater quantity by responsible cells. Meanwhile, unprimed macrophages showed no apparent cytotoxicity but induced a small secretion of IL-1β and IL-6 but greater secretion of TNFα at high PEG-GNS concentration (10 nM). This finding is similar to the results by Trickler *et al.* where NP induced TNFα production in non-tumor rat brain microvessel ECs.[33] It is possible that cells loaded with large dose of NPs may lead to reactive oxygen species (ROS) formation and cause lysosomal disruption.[34] Lysosomal disruption is one signal that activates NLRP3 and this process has been implicated in signaling inflammasome activation in many reports where the trigger is nanomaterial.[35] Nonetheless, although GNS exposure to "unprimed" macrophages did not alter cell viability, exposure to "primed" macrophages did decrease cell viability. It is therefore important to study the immunotoxicology profile before actual clinical applications.

Meanwhile, based on the response from primed macrophage, it is possible that exposing large dose NP to tumor neovasculature may exacerbate the already inflamed tumor microenvironment. Low-energy photothermal treatment, although may not induce cell death, has been shown to trigger the release of the danger-associated molecular patterns.[36] Combining the effect of NP exposure and photothermal treatment, it can potentially activate the inflammasome within tumor vascular ECs whereas the release of inflammatory cytokines may further enhance the EPR effect for deeper NP penetration. The exact mechanism on photothermally triggered BBTB permeabilization, however, requires further investigation.

Conclusion

This study demonstrates that plasmonics-active theranostic GNS can be a versatile nanoplatform for brain tumor imaging and controlled delivery of GNS into tumor in pre-clinical settings. GNS could be delivered beyond the tumor vasculature and deep into the tumor parenchyma. By focusing ultrashort pulsed laser on brain tumor in mice preinjected with PEG-GNS, for the first time a proof-of-concept plasmonics-enhanced optically modulated image-guided brain tumor microvascular permeabilization was demonstrated, showing a highly spatial selective delivery of GNS into the tumor parenchyma with minimal off-target distribution. An immunological effect illustrated by inflammasome activation upon NP exposure may also contribute to the enhanced BBTB permeability. Based on these novel advances, we envision a strong translational potential on plasmonics-active theranostic gold nanostars for brain tumor molecular imaging and image-guided plasmonics-enhanced cancer therapy.

Supplementary Material

Refer to Web version on PubMed Central for supplementary material.

Acknowledgments

References

1. Muldoon LL, Soussain C, Jahnke K, Johanson C, Siegal T, Smith QR, Hall WA, Hynynen K, Senter PD, Peereboom DM, Neuwelt EA. J Clin Oncol. 2007; 25:2295–2305. [PubMed: 17538176]

2. Krol S, Macrez R, Docagne F, Defer G, Laurent S, Rahman M, Hajipour MJ, Kehoe PG, Mahmoudi M. Chem Rev. 2013; 113:1877–1903. [PubMed: 23157552]

3. Gabathuler R. Neurobiol Dis. 2010; 37:48–57. [PubMed: 19664710]

4. Stenehjem DD, Hartz AMS, Bauer B, Anderson GW. Future Med Chem. 2009; 1:1623–1641. [PubMed: 21425983]

5. Srikanth M, Kessler JA. Nat Rev Neurol. 2012; 8:307–318. [PubMed: 22526003]

6. Liu Y, Lu W. Expert Opin Drug Deliv. 2012; 9:671–686. [PubMed: 22607535]

7. Khlebtsov N, Dykman L. Chem Soc Rev. 2011; 40:1647–1671. [PubMed: 21082078]

8. Almeida JPM, Chen AL, Foster A, Drezek R. Nanomedicine. 2011; 6:815–835. [PubMed: 21793674]

9. Condeelis J, Weissleder R. Cold Spring Harb Perspect Biol. 2010; 2:a003848. [PubMed: 20861158]

10. Vo-Dinh T, Fales AM, Griffin GD, Khoury CG, Liu Y, Ngo H, Norton SJ, Register JK, Wang HN, Yuan H. Nanoscale. 2013; 5:10127–10140. [PubMed: 24056945]

11. Xia Y, Li W, Cobley CM, Chen J, Xia X, Zhang Q, Yang M, Cho EC, Brown PK. Acc Chem Res. 2011; 44:914–924. [PubMed: 21528889]

12. Dreaden EC, Alkilany AM, Huang X, Murphy CJ, ElSayed MA. Chem Soc Rev. 2012; 41:2740–2779. [PubMed: 22109657]

13. Terentyuk, GS.; Maksimova, IL.; Dikht, NI.; Terentyuk, AG.; Khlebtsov, BN.; Khlebtsov, NG.; Tuchin, VV. Lasers for medical applications: Diagnostics, therapy and surgery. Jelinkova, H., editor. Woodhead Publishing Ltd; Cambridge: 2013. p. 659-703.

14. Yuan H, Liu Y, Fales AM, Li Y, Liu J, Vo-Dinh T. Anal Chem. 2013; 85:208–212. [PubMed: 23194068]

15. Yuan H, Khoury CG, Wilson CM, Grant GA, Vo-Dinh T. Nanotechnology. 2012; 23:075102. [PubMed: 22260928]

16. Yuan H, Fales AM, Vo-Dinh T. J Am Chem Soc. 2012; 134:11358–11361. [PubMed: 22734608]

17. Wang Y, Black KC, Luehmann H, Li W, Zhang Y, Cai X, Wan D, Liu SY, Li M, Kim P, Li ZY, Wang LV, Liu Y, Xia Y. ACS Nano. 2013; 7:2068–2077. [PubMed: 23383982]

18. Dam DHM, Lee JH, Sisco PN, Co DT, Zhang M, Wasielewski MR, Odom TW. ACS Nano. 2012; 6:3318–3326. [PubMed: 22424173]

19. Xia J, Chatni MR, Maslov K, Guo Z, Wang K, Anastasio M, Wang LV. J Biomed Opt. 2012; 17:050506. [PubMed: 22612121]

20. Yuan H, Khoury CG, Wilson CM, Grant GA, Bennett AJ, Vo-Dinh T. Nanomedicine: NBM. 2012; 8:1355–1363.

21. Hobbs SK, Monsky WL, Yuan F, Roberts WG, Griffith L, Torchilin VP, Jain RK. Proc Natl Acad Sci U S A. 1998; 95:4607–4612. [PubMed: 9539785]

22. Ye D, Raghnaill MN, Bramini M, Mahon E, Aberg C, Salvati A, Dawson KA. Nanoscale. 2013; 5:11153–11165. [PubMed: 24077327]

23. Pasha S, Gupta K. Expert Opin Drug Deliv. 2010; 7:113–135. [PubMed: 20017662]

24. Chen Y, Liu L. Adv Drug Delivery Rev. 2012; 64:640–665.

25. Liu HL, Yang HW, Hua MY, Wei KC. Neurosurg Focus. 2012; 32:E4. [PubMed: 22208897]

26. Choi M, Ku T, Chong K, Yoon J, Choi C. Proc Natl Acad Sci U S A. 2011; 108:9256–9261. [PubMed: 21576460]

27. Boulais E, Lachaine R, Hatef A, Meunier M. J Photochem Photobiol, C. 2013; 17:26–49.

28. Baffou G, Quidant R. Laser Photonics Rev. 2013; 7:171–187.

29. Melancon MP, Elliott AM, Shetty A, Huang Q, Stafford RJ, Li C. J Controlled Release. 2011; 156:265–272.

30. Lunov O, Syrovets T, Loos C, Nienhaus GU, Mailänder V, Landfester K, Rouis M, Simmet T. ACS Nano. 2011; 5:9648–9657. [PubMed: 22111911]

31. Winter M, Beer HD, Hornung V, Krämer U, Schins RPF, Förster I. Nanotoxicology. 2011; 5:326–340. [PubMed: 20846021]

32. Yang EJ, Kim S, Kim JS, Choi IH. Biomaterials. 2012; 33:6858–6867. [PubMed: 22770526]

33. Trickler WJ, Lantz SM, Murdock RC, Schrand AM, Robinson BL, Newport GD, Schlager JJ, Oldenburg SJ, Paule MG, Slikker W, Hussain SM, Ali SF. Toxicol Sci. 2010; 118:160–170. [PubMed: 20713472]

34. Carlson C, Hussain SM, Schrand AM, Braydich-Stolle LK, Hess KL, Jones RL, Schlager JJ. J Phys Chem B. 2008; 112:13608–13619. [PubMed: 18831567]

35. Jin C, Flavell RA. J Clin Immunol. 2010; 30:628–631. [PubMed: 20589420]

36. Nguyen HT, Tran KK, Sun B, Shen H. Biomaterials. 2012; 33:2197–2205. [PubMed: 22177288]
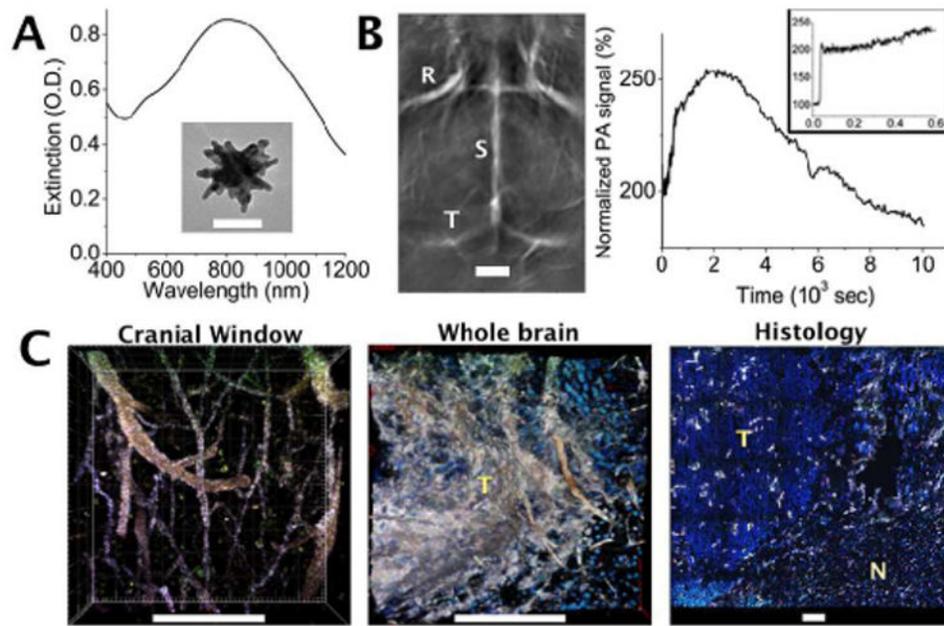
Fig. 1.
(A) Plasmon band extinction spectrum and TEM image of GNS. Scale bar: 50 nm. (B) PACT image acquired through an intact mouse scalp after PEG-GNS injection. R: rostral rhinal vein. S: sagittal sinus. T: transverse sinus. Scale bar: 2 mm. PA intensity (normalized to the 1st frame) of sagittal sinus calculated from each frame. The small jerk at 600 second was due to system transition. (inset) Normalized PA intensity monitored for the initial 600 seconds. (C) MPM imaging of cerebral microangiogram, Hoescht 33342-stained whole brain, and DAPI/CD31-stained histology. GNS are white. T: tumor. N: normal. Scale bar: 200 μm.
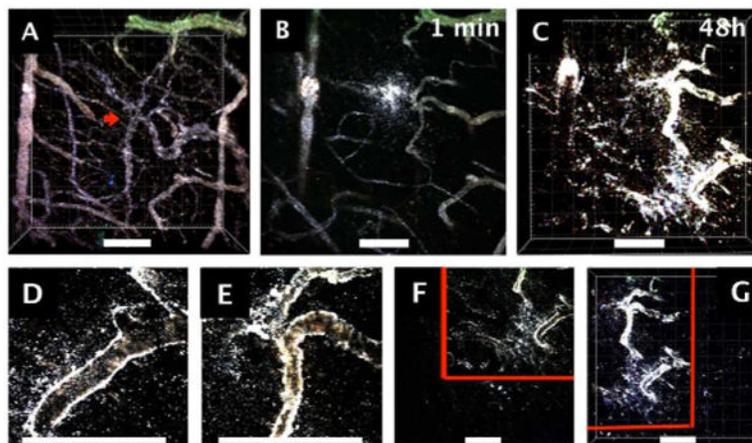
Fig. 2.
MPM images of photothermal-triggered tumor BBTB permeation examined through a cranial window. Tumor vessels prior to (A), 1-min after (B), and 48-hr after (C-G) laser irradiation. Following the irradiation, PEG-GNS (white) were found residing near the blood vessels and extravasating deep into the parenchyma (D,E), but not outside the irradiation zone (F,G). Red arrow denotes vascular tortuosity; red lines denote the border of irradiation. Scale bar: 100 μm.
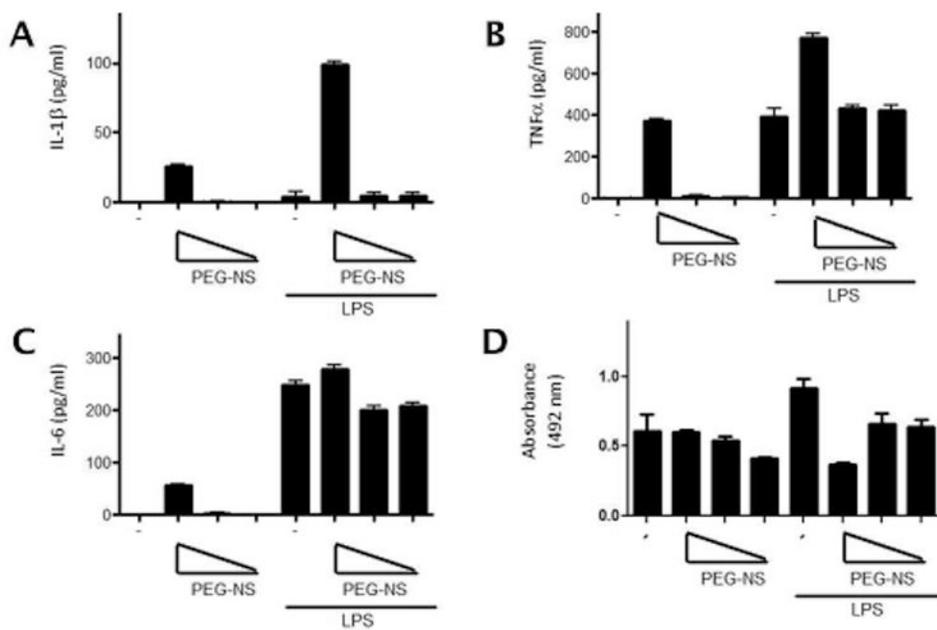
Fig. 3.
Cytokines induction (IL-1β [A], TNFα [B], IL-6 [C]), and cytotoxicity (D) profiles from LPS-primed and unprimed BMDMS treated with PEG-GNS for 24 hours. Triangles denote PEG-GNS concentration of roughly 10, 1, 0.1 nM. Error bar: 1 SD.